COBEM 2023 27TH INTERNATIONAL CONGRESS OF MECHANICAL ENGENEERING

ABCM Brazilian Society of Mechanical Sciences and Engineering
27th ABCM International Congress of Mechanical Engineering
December 04-08, 2023, Florianópolis-SC, Brazil

COB-2023-0221
COMPUTATIONAL ANALYSIS OF THE EFFECT OF WAVY LEADING EDGE ON STABILIZER

Pablo Gonzalez-DeGreiff
William Gomez-Rivera
New Granada Military University (UMNG), Cajicá, Cundinamarca, Colombia.
est.pablo.gonzalez@unimilitar.edu.co
william.gomezr@unimilitar.edu.co

Pedro David Bravo-Mosquera
Hernan D. Cerón-Muñoz
São Carlos School of Engineering, University of São Paulo (EESC / USP), São Carlos, SP, Brazil, 13563-120.
pdbravom@usp.br
hernan@sc.usp.br

Abstract. *Wavy Leading Edge (WLE) is a bio-mimetic device inspired by the tubercles found on humpback whales. Generated by a sinusoidal function, they alter the flow field around the airfoil by increasing its momentum exchange and airfoil surface suction. Lately, there has been an increased interest in the topic; but despite that, few studies have addressed the performance effects of WLE applied to a stabilizer. This article aims to evaluate and demonstrate this possible application through the use of numerical simulations at a Reynolds number of* 3×10^6 *and a Mach number of 0.35. Block-structured hexahedral meshes of a NACA 0012 modified stabilizer were simulated and compared using the Reynolds-averaged Navier-Stokes (RANS) equations with the* $k-\omega$ *SST (Shear-Stress Transport) turbulence model. Both the wavy leading edge geometry variation, as well as the effect of altering the angle between peaks and flow direction, were evaluated. To perform this, the aerodynamic coefficients were measured for each of the six selected models; along with surface pressure coefficients and turbulence kinetic energy contours. The* $A = 0.03c$ *and* $\lambda = 0.414c$ *configuration showed a reduced pitching moment for* $C_L < 0.5$ *of around 10% less and a slightly steeper lift slope of around 3% higher. It was found that varying the tubercles angle with respect to the flow has a substantial effect, tubercles perpendicular to the leading edge showed a* C_{Lmax} *decrease of as much as 6.3% lower. WLE could potentially reduce the structural loads in stabilizers, while slightly increasing their performance with minimal drag penalties.*

Keywords: *Wavy Leading Edge, WLE, Leading-edge tubercles, leading-edge protuberances, Stabilizer*

1. INTRODUCTION

Lately, current studies have a tendency to gravitate to bio-mimicry. Nature has been a key source of inspiration for mankind, with its millions of well-coordinated algorithms and processes, as well as its enormous array of finely made species and materials. One example of these research topics that emerged from this, particularly, in the field of aerodynamics and flow control; is the performance effects of introducing leading-edge protuberances in both airfoils as well as hydrofoils. These devices, in recent research studies, have been given the name of Wavy Leading Edge (WLE) and are inspired by the tubercles found on the leading edge of pectoral flippers of the humpback whale (*Megapteranovaeangliae*), which despite their vast size, are surprisingly agile in comparison to other whales. It has been proposed that their agility is due in part to the usage of pectoral flippers (Fish, 1999; Fish and Battle, 1995), these protuberances found on the leading edge alter the flow field around the whale's airfoil-like flipper, allowing it to remain attached for a larger range of attack angles, thus maintaining lift; whereas without them, the flipper would stall much sooner. In some cases, it has also been shown by some researchers that tubercles improve drag, or at least incur minor drag penalties when used. (Watts *et al.*, 2001; Miklosovic *et al.*, 2004). As a result, throughout the last decade, there has been a lot of interest in studying the performance implications of Wavy Leading Edge on airfoils and hydrofoils. A number of scholars have postulated and empirically demonstrated (Watts *et al.*, 2001; Miklosovic *et al.*, 2004) several mechanisms responsible for performance enhancement, not always operating as a single reason, but virtually always working together in more sophisticated ways.

Generally speaking, the mechanisms behind the performance improvement can be broadly classified as follows: generation of stream-wise vortices that increase boundary layer momentum exchange (Miklosovic *et al.*, 2004; Custodio, 2007; Fish and Battle, 1995; Johari *et al.*, 2007), minimization of span-wise stall progression through compartmentalization of the flow (Fish and Battle, 1995; Miklosovic *et al.*, 2007), alteration of pressure distribution along the airfoil (Dropkin *et al.*, 2012; Favier *et al.*, 2012), and vortex lift analogous to swept and delta wings (Custodio, 2007; Miklosovic *et al.*,

2007). The various explanations of why introducing protuberances on the leading edge may be beneficial may be due to the various Reynolds numbers tested throughout the research papers, Hansen *et al.* (2010) proposed that one of the most critical factors to consider when evaluating the performance effects of WLE is the Reynolds number since it seems that below $Re = 3 \times 10^5$ the tubercles show detrimental effects, while at $Re \geq 5 \times 10^5$ the contrary is shown. Furthermore, Custodio (2007) found that past a Reynolds number of $Re = 3.6 \times 10^5$ the aerodynamic forces exhibit little to no dependency on the variation of the Reynolds number, which was later confirmed by Dropkin *et al.* (2012), who obtained comparable results.

Other factors to consider include sweep angle, Custodio (2007) found that modified swept wings never manage to outperform the baseline airfoils since the addition of tubercles improves lift in the post-stall regime but at the same time, also increases drag; thus, the lift-to-drag ratio never surpasses the unmodified airfoil. Later Joseph *et al.* (2019) reinforced this by suggesting that introducing WLE in swept wings is not as beneficial as in straight wings since it seems the counter-rotating streamwise vortices pairs (CVPs) formed by the tubercles appear to be broken down by the span-wise flow caused by the sweep angle. On the contrary, Hansen *et al.* (2010) suggests that tubercles may be more beneficial in swept and/or taper wings since there is a larger amount of spanwise flow present and it has been suggested by Miklosovic *et al.* (2007) that the success of tubercles is due in part to minimization of span-wise stall progression.

The amplitude and wavelength of the tubercles are crucial in determining how they will alter the wake topology, flow recirculation zones, and the strength of the wake vortex shedding. Several parametric studies, like one performed by Favier *et al.* (2012) and another by Chen *et al.* (2020) have studied the effect of said parameters, the latter proposed that the WLE with the greatest amplitude and shorter wavelength performs the worst, and the former discovered that at a specific configuration of $A = 0.07c$ and $\lambda = 1c$, the wake vortex shedding is reduced, and an almost quasi-steady wake is obtained, resulting in a reduction in fluctuations in the aerodynamic forces and a reattachment of the flow. Another parametric study performed by Johari *et al.* (2007) revealed that the best overall performance was obtained with a smaller amplitude configuration of $A = 0.025c$, although the wavelength had little influence on the aerodynamic forces. This corroborates what has previously been found by past authors, it seems that there is an optimal amplitude-to-wavelength ratio (A/λ) depending on each wing configuration that produces the best results, a statement that Hansen *et al.* (2011) also proposed, by finding out that the smallest amplitude and shorter wavelength configuration ($A03\lambda11$) with a A/λ ratio of 0.27 performed the best.

Wing tip condition may be another important factor to consider when analyzing WLE performance effects, Miklosovic *et al.* (2007) found that on infinite span wings, the streamwise vortices generated by the WLE caused early separation whereas, on a finite span wing, these vortices minimize spanwise stall progression by compartmentalization of the flow; phenomena also seen by Custodio (2007), where he postulated that protuberances essentially act as fences directing flow in the chord-wise direction thus inhibiting to some extent the creation of wingtip vortices, consequently reducing induced drag and increasing lift. Besides considering the wing as having a finite span, another important factor may be the aspect ratio (AR); Chen *et al.* (2012) tested various wings with varying aspect ratios and found out that for wings with lower $AR = 1$, the stall delay improvement was more noticeable than in higher AR wings. Recently Yang *et al.* (2023) conducted a study in which the influence of WLE in low aspect ratio wings proved effective at delaying stall and reducing wake vortex shedding, using two-dimensional time-resolved particle image velocimetry (TR-PIV).

Another critical factor is the spanwise flow caused by the pressure gradient slightly behind the leading edge. As demonstrated by Skillen *et al.* (2015), who also found the presence of a secondary flow in which the low-inertia fluid behind the peak flows into the valley, and thus pulls high-momentum fluid drawn from above. This causes a re-energization of the boundary layer and a cyclic variation of spanwise vortices, which in turn generates pairs of counter-rotating streamwise vortices (CVPs). Therefore, this helps to maintain the boundary layer attached for higher angles of attack; thus increasing the overall operating envelope. Various authors have described this same phenomenon, Perez-Torro and Kim (2017) performed a numerical study and observed the evolution of CVPs. They found that each CVP being formed behind each peak acts as a buffer zone between the adjacent fully separated shear layers (SSL) and the laminar separation bubbles (LSBs) formed behind the troughs. Wavelength played a major role in determining the strength of this effect. Yang *et al.* (2023) observed too the same CVPs in low aspect ratio wings, as did Chen and Wang (2014) on delta wings using stereoscopic particle image velocimetry (SPIV).

The aim of this research is to look into one of the potential applications of WLE, which could provide significant aerodynamic improvements when applied to a stabilizer. The flow mechanism has already been studied extensively; nevertheless, few real-world aeronautical applications have been investigated. The current hypothesis proposed by the authors of the present study is that by implementing this bio-mimetic device the performance of the stabilizer could be improved. Towards this end, the present experiments encompass several numerical simulations based on Reynolds-averaged Navier-Stokes (RANS) equations at Reynolds number of 3×10^6, and angles of attack up to $\alpha = 25°$. The planform selected was that of the vertical stabilizer of the agricultural aircraft (AG-NEL 25) (Bravo-Mosquera *et al.*, 2018) which uses the symmetrical NACA 0012 airfoil profile. The overview of the geometrical parameters is described in Section 2, the numerical method is presented in Section 3, the results are presented and discussed in Sections 4. and 5. respectively, and finally the findings are summarized in Section 6.

2. WLE GEOMETRY AND DESIGN

In order to study the effect of the protuberances, their geometry must be defined first. The leading edge waviness is introduced by modifying the local chord length periodically along the spanwise direction, this is modelled using a sinusoidal equation, which according to Favier *et al.* (2012) is the following:

$$f(z) = A \cdot c \cdot \cos\left(z \cdot \frac{2\pi}{\lambda \cdot c}\right), \tag{1}$$

where A, λ and c are the tubercle amplitude, wavelength, and chord respectively. Figure 1a shows the undulated leading-edge control parameters described previously.

Using Eq. (1) as a basis, an own equation is derived, the first modification is varying the amplitude A and the wavelength λ with the local chord C_l, for this, the chord c must be expressed as a function of z, taking the x axis in the stream-wise direction, and the z axis normal to the free-stream direction the Eq. (2) is derived,

$$c_l(z) = \left(c_r - \frac{c_r - c_t}{s} \cdot z\right), \tag{2}$$

where c_r is the root chord, c_t is the tip chord, and s is the wing span.

The next modification is to introduce asymmetricity, this is accomplished by adding an implicit vertical linear equation expressed by Eq. (3) to the z term of Eq. (1), doing so adds positive skewness for all $\Theta > \Lambda$ and negative skewness for all $\Theta < \Lambda$, Fig. 1b illustrates this. Previous researchers (Flores Mezarina *et al.*, 2019) have also studied the effects of introducing asymmetricity, however, it was done in straight wings and a different method was used. This study provides an alternative method that has the advantage of having the angle between peaks and flow direction as a control parameter, and unlike prior methods employed, the sine function does not tend to a saw-tooth wave at large angles of asymmetry.

$$\gamma(x) = \tan(\Theta - \Lambda) \cdot x, \tag{3}$$

where Θ is the peak skewness angle with respect to the flow and Λ is the leading edge sweep angle.

A linear transformation is done in order to allow for a sweep angle (Λ), this basically means rotating both axes, as seen in Eqs. (5). The term π is subtracted in order to start the waviness on a function zero with a peak at the start. This ensures a constant root chord independent of the control parameters chosen. Finally, the following implicit WLE equation is obtained which in turn produces the leading-edge curve $f(z)$ shown in Fig. 1c,

$$x_r(x,z) = \frac{A \cdot c_l(z)}{2} \cdot \sin\left((y_r(x,z) + \gamma(x)) \cdot \frac{2\pi}{\lambda \cdot c_l(z)} - \pi\right), \qquad 0 \le z \le s \tag{4}$$

where Eqs. (5).

$$x_r(x,z) = [x \cdot \cos(\Lambda) - z \cdot \sin(\Lambda)], \qquad y_r(x,z) = [x \cdot \sin(\Lambda) + z \cdot \cos(\Lambda)] \tag{5}$$

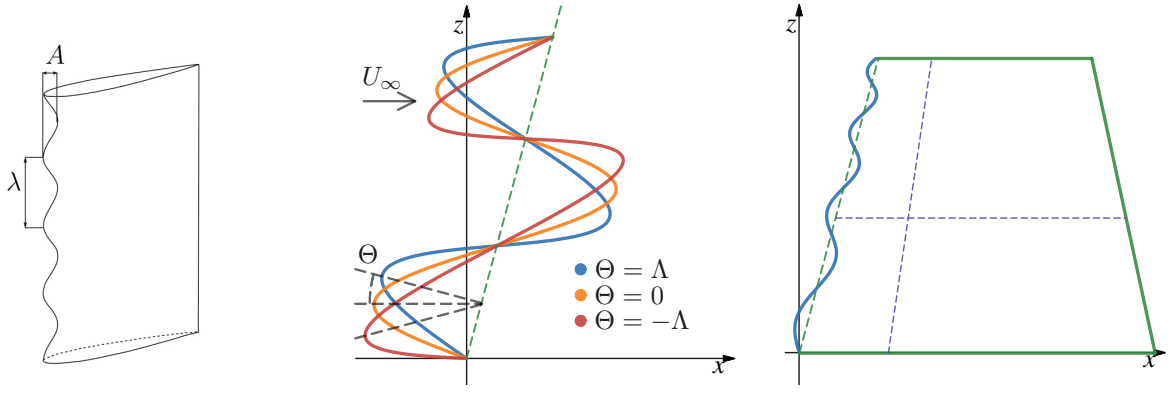

(a) (b) (c)

Figure 1: (a) WLE Geometry Parameters, adapted from Favier *et al.* (2012), (b) Sine skewness, when $\Theta = \Lambda$ the peaks are perpendicular to the leading edge, and when $\Theta = 0$ they are parallel to the flow, (c) Wing planform.

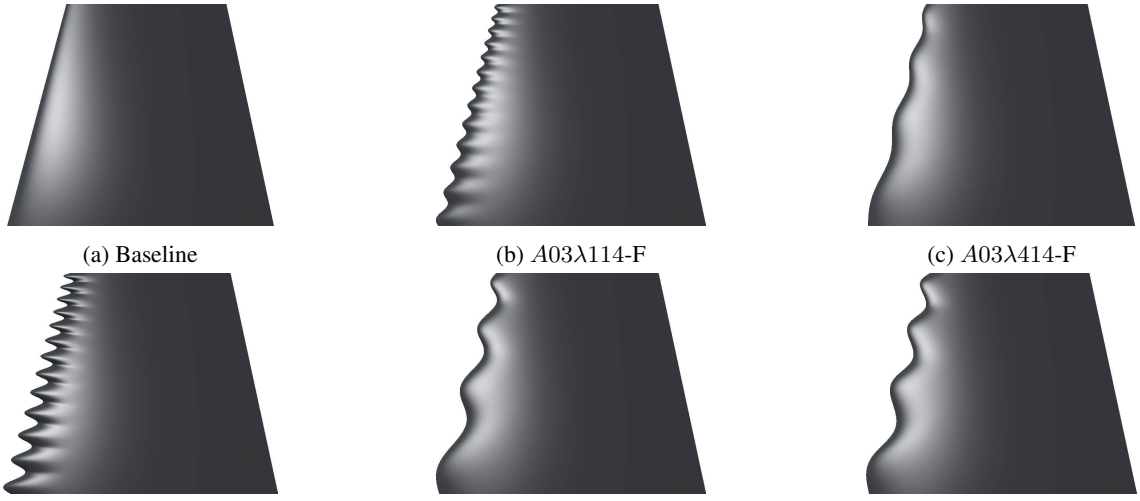

(a) Baseline (b) $A03\lambda114$-F (c) $A03\lambda414$-F

(d) $A07\lambda114$-F (e) $A07\lambda414$-F (f) $A07\lambda414$-LE

Figure 2: Wing models.

Table 1: Model Parameters and Names.

Model Name	Parameters	Model Name	Parameters	Model Name	Parameters
Baseline	$c_r = 490$ mm $c_t = 294$ mm $s = 405.72$ mm $\Lambda = 15.0$ deg	$A03\lambda114$-F	$A = 0.03$ $\lambda = 0.114$ $\Theta = 0.0°$ $A/\lambda = 0.26$	$A03\lambda414$-F	$A = 0.03$ $\lambda = 0.414$ $\Theta = 0.0°$ $A/\lambda = 0.07$
$A07\lambda114$-F	$A = 0.07$ $\lambda = 0.114$ $\Theta = 0.0°$ $A/\lambda = 0.61$	$A07\lambda414$-F	$A = 0.07$ $\lambda = 0.414$ $\Theta = 0.0°$ $A/\lambda = 0.17$	$A07\lambda414$-LE	$A = 0.07$ $\lambda = 0.414$ $\Theta = 15.0°$ $A/\lambda = 0.17$

2.1 Wing Models

With the Leading-Edge curve defined by Eq. (4) and the vertical stabilizer planform based from Bravo-Mosquera *et al.* (2018), the wing models shown in Fig. 2 were created using the CAD Onshape. The loft is created between the root NACA 0012 airfoil profile and the tip with the same profile; using as guides both the leading-edge curve defined with Eq. (4), and two straight lines connecting both airfoil profiles at 25% of the chord, ensuring that behind this point the wing remains unchanged by the waviness when compared to the baseline configuration. Table 1 summarizes all the model parameters. The naming convention of the models corresponds to their Amplitude, their wavelength denoted by λ, both followed by their value after the decimal; and a designator at the end, indicating if the tubercles are parallel to the flow (F) or perpendicular to the leading-edge (LE); this is controlled by the value of Θ.

The A/λ ratio was chosen based on the study performed by Hansen *et al.* (2011) who observed that the maximum lift coefficient, largest stall angle, and lowest drag were achieved by a $A/\lambda \approx 0.27$. The configurations tested were chosen based on both the results obtained by Favier *et al.* (2012); who reported that the highest performance was obtained when $A = 0.07c$, and the configuration that Hansen *et al.* (2011) proposed showed the best results. Combining the two amplitudes, and the two wavelengths, four models are obtained ($A07\lambda414$-F, $A03\lambda114$-F, $A07\lambda114$-F, $A03\lambda414$-F). One additional configuration ($A07\lambda414$-LE) was studied which had its tubercles perpendicular to the leading edge ($\Theta = \Lambda$).

3. NUMERICAL METHOD

In order to perform the computational fluid dynamics (CFD) study, the steady-state Reynolds-averaged Navier-Stokes (RANS) equations were used. Under the constant property, incompressible flow assumption they were discretized using the finite volume method; according to the numerical methodology implemented in Ansys® CFX, Release 18.1 Ansys (2017). The $k - \omega$ SST (Shear-Stress Transport) turbulence model was chosen since according to Steed (2011) it can better predict the turbulence effects and Hansen *et al.* (2016) found it capable of capturing the flow characteristics of WLE.

3.1 Computational domain and boundary conditions

For this study, a rectangular domain topology, with a double domain interface containing an inner O-grid cylindrical hexahedral mesh was used. Selecting similar domain boundary lengths as Hassan *et al.* (2015); Hansen *et al.* (2016), a computational fluid domain shown in Fig. 3a was created, here the boundary distances as a function of the chord can be appreciated. An inner secondary cylindrical domain with twelve chord lengths ($12c$) diameter was created with the purpose of not having to create multiple meshes for each varying angle of attack. Allowing for the change of angle of attack by rotating the inner mesh while maintaining constant values for the free-stream velocity components. The wing surface was assigned the no-slip boundary condition, all the walls were set as ideal with free-slip, and the interface between domains was set as fluid-fluid with General Grid Interface (GGI). All meshes are of block-structured hexahedral topology, consisting of around 3.3×10^6 cells. Near-wall cells are placed at $y^+ < 1$ everywhere with a growth ratio not exceeding 20%. The high-resolution advection scheme was used and the convergence criteria were set towards reaching a hundred iterations with maximum residual values of RMS $= 1.0 \times 10^{-5}$.

3.2 Mesh sensitivity study

Maintaining the same blocking structure, three different meshes were considered in order to evaluate their influence on the results, each one varying in element size; these can be seen in Tab. 2. Starting with 1.5M elements, each mesh doubles in size up to 7.0M elements. Each one was simulated at zero angles of attack ($\alpha = 0$), with the following flow conditions: Reynolds number of 3×10^6, inlet free-stream velocity (U_∞) of 120 m/s (Mach = 0.35), and the domains were set as air at 25° Celsius. The resulting drag coefficient was used as a convergence criterion. Three quality criteria were evaluated for the mesh creation, minimum determinant 3x3x3, angle, and quality. All the final selected meshes had a determinant 3x3x3 higher than 0.67. Table 2 summarizes these results, the calculated drag coefficient in the coarse and medium meshes varied 22.6%, while between the medium and fine meshes, it varied 2.8%. Since the variation was less than 5% between the latter, the medium mesh was selected since it offers the most accurate results with the least computational cost.

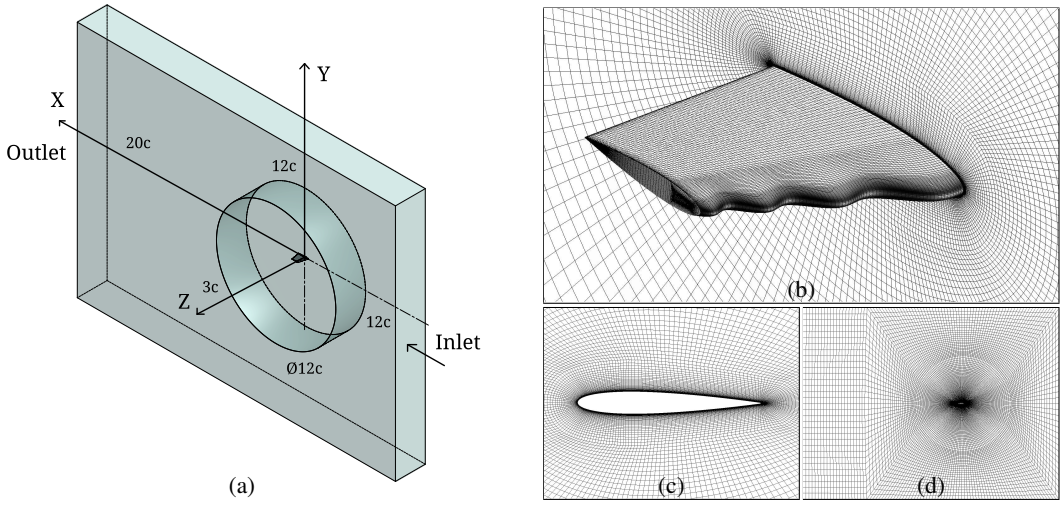

Figure 3: (a) Computational domain, (b) Structured mesh surface detail, (c) Structured mesh root chord profile view, (d) Double domain interface complete view.

Table 2: Meshes for Sensitivity Study.

Mesh	Elements	Determinant 3x3x3	Angle	Quality	C_D	ΔC_D
Coarse Mesh (1.5M)	1,559,484	(Min 0.630 Max 0.999)	(Min 19.71 Max 89.82)	(Min 0.337 Max 0.998)	0.0121	22.627%
Medium Mesh (3.3M)	3,354,043	(Min 0.671 Max 0.999)	(Min 19.80 Max 89.91)	(Min 0.338 Max 0.999)	0.0099	–
Fine Mesh (7.0M)	7,022,452	(Min 0.682 Max 1.000)	(Min 19.80 Max 89.91)	(Min 0.339 Max 0.999)	0.0096	2.801%

4. RESULTS

Presented in Fig. 4 are the results of various steady-state simulations carried out at a $Re = 3 \times 10^6$ and Mach = 0.35 (120 m/s) up to $\alpha = 25°$. Pressure coefficients and contours are presented in Fig. 5 and discussed subsequently. The goal of this study is to assess the performance effects of a stabilizer with WLE and to identify the potential benefits of its application. In order to do so, the aerodynamic force coefficients were studied, with particular emphasis on the moment coefficient and its derivative with respect to the lift coefficient.

4.1 Effect of Amplitude

The lift coefficient curve for all configurations is presented in Fig. 4a. All wings, with the exception of ($A07\lambda114$-F), present a linear increase in lift up until $\alpha = 18°$. The baseline configuration lift coefficient keeps increasing steadily up until $\alpha = 22°$, reaching a C_{Lmax} of 1.04. Afterwards, it abruptly falls and then rises again. The configuration with the largest amplitude and longest wavelength ($A07\lambda414$-F) follows the baseline lift slope up until $\alpha = 19°$, reaching a C_{Lmax} of 0.87 and then reduces to a plateau at $C_L \approx 0.7$. Meanwhile, the models with lower amplitude see a higher C_{Lmax} of 0.9 and subsequently fall to a similar plateau, although with a steeper drop.

When compared to the baseline foil, the C_{Lmax} drops by as much as 16.2% for the tubercles with $A = 0.07$, and 11.8% when $A = 0.03$. Indicating an inverse relationship between amplitude and C_{Lmax}. Conversely increasing the amplitude marginally smooths out the post-stall behaviour, this goes in accordance with the findings made by Hansen *et al.* (2011). Oppositely to what other authors have found (Fonseca *et al.*, 2021; De paula *et al.*, 2017, 2018) it seems WLE do not increase considerably the C_{Lmax} in this particular configuration. Figure 4b plots the drag coefficient curve.

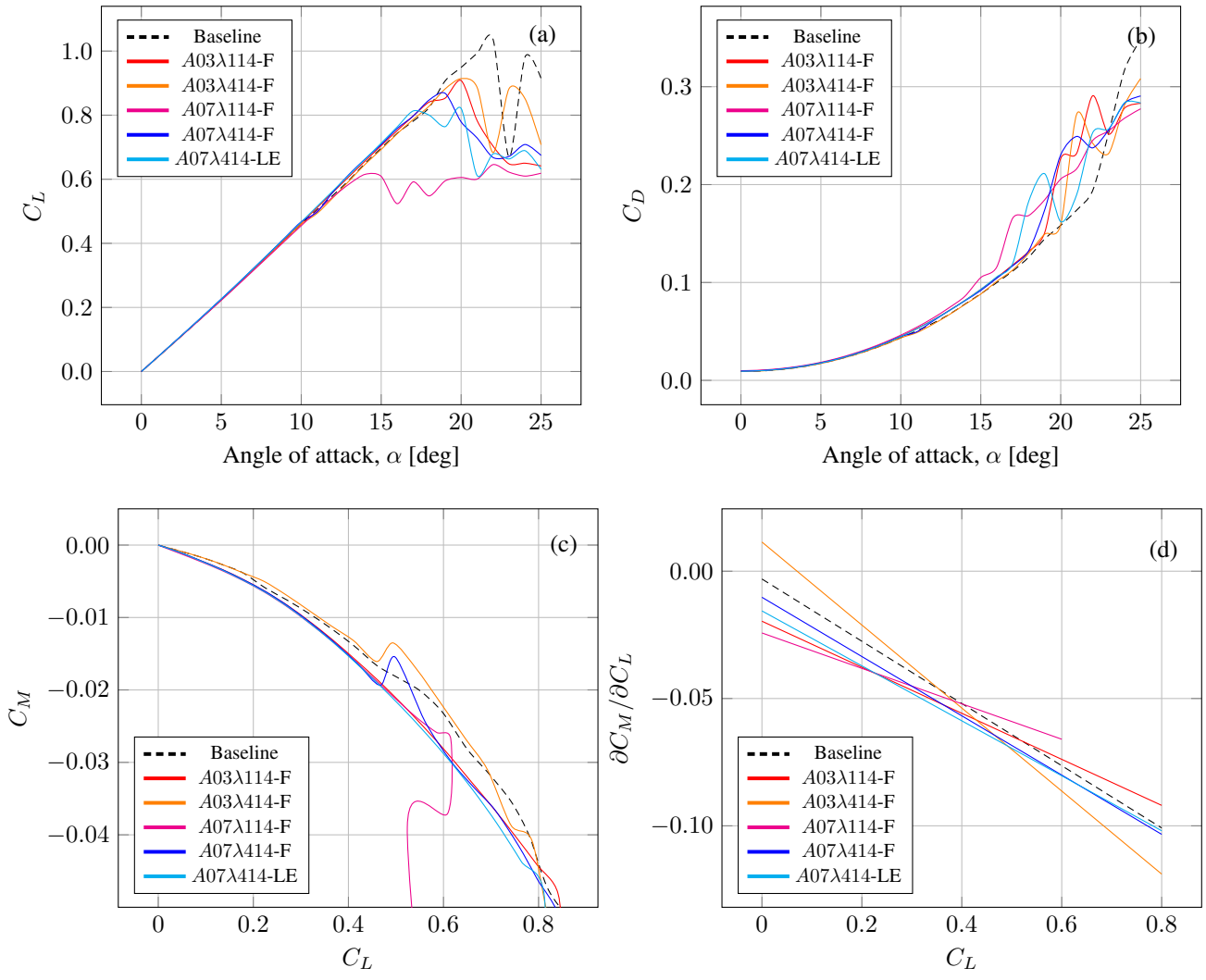

Figure 4: (a) Lift coefficient (C_L) vs. angle of attack (α), (b) Drag coefficient (C_D) vs. angle of attack (α), (c) Moment coefficient (C_M) vs. lift coefficient (C_L), (d) Moment coefficient derivative with respect to lift coefficient ($\partial C_M/\partial C_L$) vs. C_L.

As a direct consequence of the fact that configurations with higher amplitude achieve a lower C_{Lmax}, but present an earlier although smoother stall onset; there is an increase in drag associated with the increment in amplitude. When compared to the baseline unmodified foil, the configuration with the lowest amplitude, and longest wavelength ($A03\lambda414$-F) shows drag values equal or better during the linear lift curve slope up until $\alpha = 15°$. Meanwhile, configurations with greater amplitudes show an increase in drag of up to 5.7% more in the same interval ($0° \leq \alpha \leq 15°$). Owing to the fact that for modified wings the stall comes more gradually, and starts behind the troughs at lower angles of attack.

The slope of the linear range in the lift curves ($\partial C_L/\partial\alpha$) up until $\alpha = 18°$ was measured for each configuration. All modified wings, except the one with the highest A/λ ratio ($A07\lambda114$-F), exhibited a minor increase in their lift slope of roughly 3% when compared to the baseline configuration. Pressure coefficient and wall shear stress measurements confirmed this was not due to the presence of separation bubbles. The unmodified foil had a $\partial C_L/\partial\alpha$ of 0.046, whereas $A07\lambda414$-F had the highest lift slope of 0.048.

4.2 Effect of Wavelength

The aerodynamic efficiency of all the configurations remains fairly similar at least for the linear range. All models tested have their maximum L/D ratio at $\alpha = 5°$. Compared to the unmodified foil, the foil with the longest wavelength and smallest amplitude ($A03\lambda414$-F) has a similar maximum L/D of 12.9. However, increasing the A/λ ratio appears to result in a decrease in the maximum L/D, since the configuration with the greatest A/λ ratio of 0.61 had 7.5% less aerodynamic efficiency than the unmodified one. This could be attributed to the reduction in wavelength, however, as Hansen *et al.* (2011) reported there could be instead an optimum amplitude-to-wavelength ratio in which the best results are obtained.

Altering the wavelength changes how evenly the streamwise counter-rotating vortex pairs (CVPs) mix the high-momentum fluid from above, replacing the lower inertia fluid located behind the peaks. Each CVP forms as a result of the pressure gradient caused by each periodic variation of the leading edge, this can be seen in the C_p contours shown in Fig. 5. A low-pressure zone forms at the trough and this causes the formation of two vortices initiated at each adjacent peak. They continue streamwise and can be identified by the low wall shear stress (τ_w) above the surface. Similarly to what Perez-Torro and Kim (2017) found, each of these streamwise vortices seems to work as a fence that not only impedes the spanwise flow but works as a barrier between the developed LSB and the adjoining shear layers. Therefore, the flow above the surface of the wing is effectively compartmentalized between each trough. Turbulence Kinetic Energy plots located in Fig. 6 help visualize how varying the wavelength affects the number of CVPs and their size. Configurations with $\lambda = 0.414c$ (Fig. 6b) seem to produce three CVPs, each one located behind each trough. CVPs vary in size according to their spanwise location; longer wavelengths appear to produce larger CVPs, while shorter wavelengths near the wingtip produce smaller ones. Configurations with $\lambda = 0.114c$ (Fig. 6c) on the other hand produce smaller, although more homogeneous CVPs behind each trough.

4.3 Pitching Moment

The pitching moment coefficient as a function of the lift coefficient, and its derivative plot are presented in Fig. 4c and Fig. 4d, respectively. Examining the pitching moment coefficient plot, there seems to be a sudden slight spike at $C_L = 0.5$, linked to the configurations with the longest wavelength. This may be due to the fact that shorter wavelength tubercles produce smaller, although closer CVPs (just as seen in Fig 6), which have a higher chance of interacting with each other. Thus, these configurations present a smoother, more thorough mixture of the boundary layer; promoting a higher momentum exchange, hence prolonging sudden fluctuations which cause these phenomena.

However for $C_L < 0.5$ configurations with longer wavelengths present a more downward concave pitching moment curve. This is evidenced by the plot in Fig. 4d, where their moment coefficient derivative shows a steeper slope indicating higher concavity. This means WLE could effectively reduce the pitching moment with minor drag penalties for lower C_L values.

4.4 Effect of Orientating the Tubercles

An additional study was conducted on varying the orientation of the tubercles with respect to the flow. Configurations ($A07\lambda414$-F) and ($A07\lambda414$-LE) are identical, except for the fact that the latter has a $\Theta = \Lambda = 15.0°$, meaning the tubercles are perpendicular to the leading edge; whereas the former has them parallel to the flow direction. The configuration with the tubercles perpendicular to the leading edge (LE) had a 6.3% lower C_{Lmax} when compared to its counterpart (F). Both variants exhibit similar linear ranges for the curve slope, however, the LE one seems to have a steeper drop in lift. Similarly, when their drag curves are compared in Fig. 4b, the (LE) configuration appears to perform worse, with an earlier onset of drag as a result of a sooner stall.

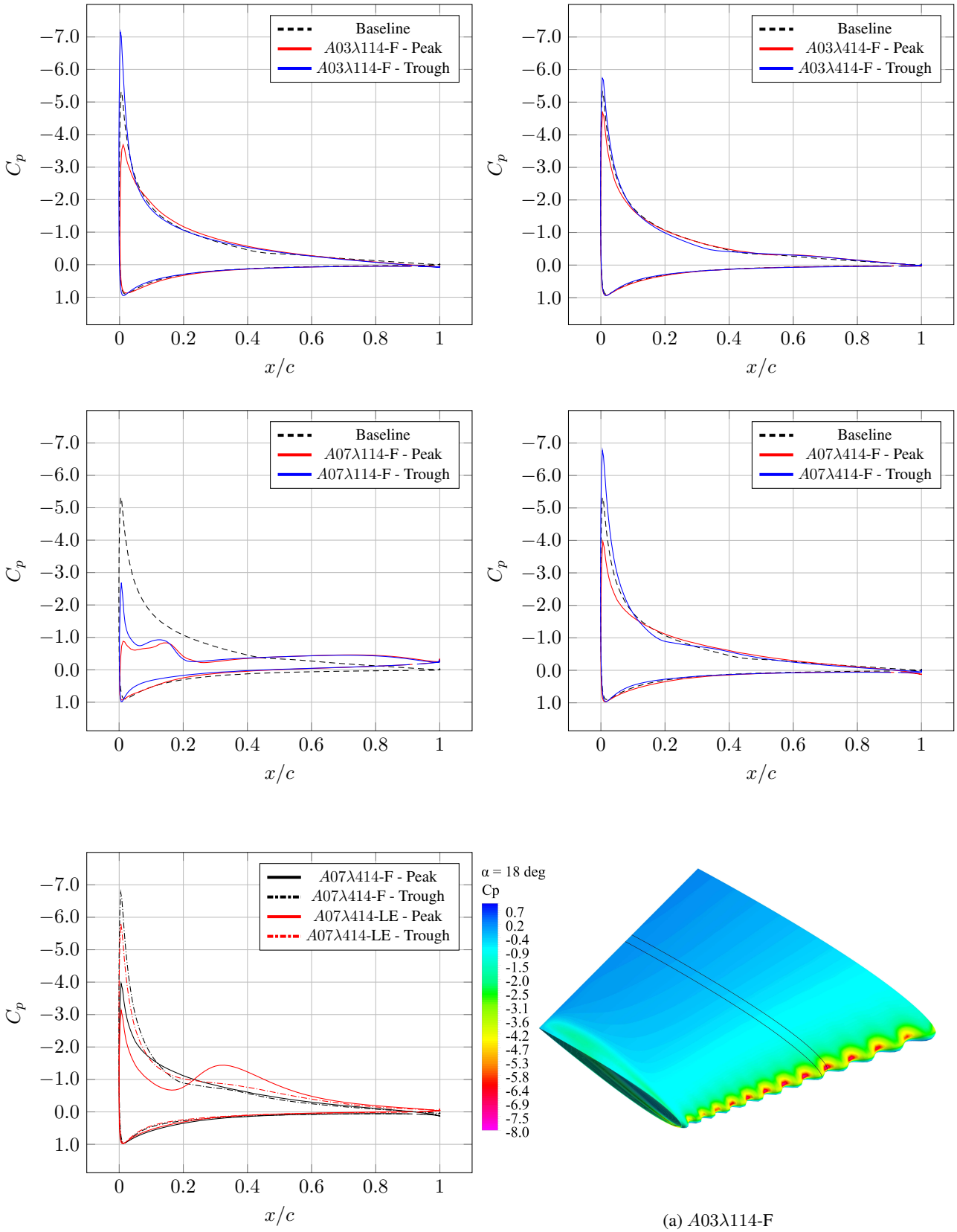

(a) $A03\lambda114$-F

Figure 5: Surface pressure coefficients along mean chord at 18 degrees angle of attack (α).

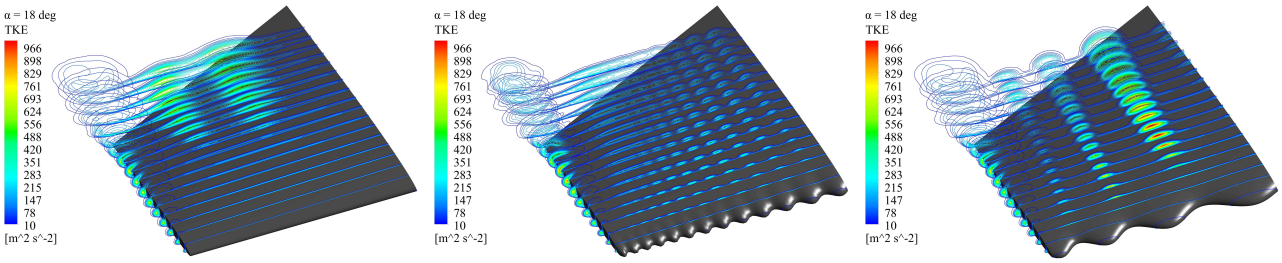

(a) Baseline (b) $A03\lambda114$-F (c) $A07\lambda414$-F

Figure 6: Turbulence Kinetic Energy (TKE) at 18 degrees angle of attack (α). Planes at $0.05c$ intervals, starting at $x/c = 0$

5. DISCUSSION

Lift and drag results presented in this study show similar behaviour to many of those reported in the introduction. Although in contrast to the study performed by Almeida Rocha *et al.* (2018), WLE does not seem to increase the C_{Lmax} considerably in this particular configuration. Instead, it seems adding WLE reduces the maximum lift, but replaces the traditional sudden stall for a smoother gradual loss of lift similar to what Hansen *et al.* (2011); Johari *et al.* (2007); Miklosovic *et al.* (2007) have reported. The tubercles seem to act as vortex generators, increasing the amount of momentum exchange across the boundary layer thanks to the CVPs they develop behind the troughs, which in turn replace the fluid behind the peaks re-energizing it. The mechanism behind WLE has already been studied a good amount, especially its benefits in the post-stall regime; however, an interesting effect of adding WLE seems to happen in the linear range too. When compared to the unmodified stabilizer, the ($A03\lambda414$-F) configuration showed a reduced pitching moment for $C_L < 0.5$ of around 10% less and a slightly steeper lift slope ($\partial C_L/\partial\alpha$) of around 3% more.

6. CONCLUSION

The effects of Wavy Leading Edge on a stabilizer were studied through the means of computational analysis. A similar behaviour to what previous authors have found explaining the mechanism behind WLE has been found. The tubercles generate counter-rotating vortex pairs (CVPs), the number of which is directly proportional to the number of tubercles or wavelength. These CVPs help to maintain the boundary layer attached for longer and improve the post-stall characteristics. The results appear to indicate that adding tubercles to a stabilizer could prove to be beneficial, as the $A = 0.03c$ and $\lambda = 0.414c$ configuration showed a reduction of in pitching moment of up to 10% for C_L less than 0.5, as well as a slight increase of around 3% in its lift curve slope. This could imply a reduction in the structural loads a stabilizer must withstand while incurring minimal drag penalties.

7. ACKNOWLEDGEMENTS

Words cannot express my gratitude to Juan Antonio Flores Mezarina who generously provided knowledge and expertise, and went above and beyond to help me with my work. Additionally, this endeavour would not have been possible without the generous support from the Inter-institutional and International Relations Office (ORI) of the New Granada Military University, which allowed me the opportunity to perform this research internship and helped finance my research.

8. REFERENCES

Almeida Rocha, F., De paula, A., Sousa, M., Cavalieri, A. and Kleine, V., 2018. "Lift enhancement by wavy leading edges at Reynolds numbers between 700,000 and 3,000,000". doi:10.2514/6.2018-3816.

Ansys, I., 2017. "ANSYS CFX-solver theory guide". *Ansys CFX Release 18.1*, Vol. 15317.

Bravo-Mosquera, P., Cerón-M, H., Díaz-Vázquez, G. and Catalano, F., 2018. "Conceptual design and CFD analysis of a new prototype of agricultural aircraft". *Aerospace Science and Technology*, Vol. 80, pp. 156–176. doi:10.1016/j.ast.2018.07.014.

Chen, H. and Wang, JJ., 2014. "Vortex structures for flow over a delta wing with sinusoidal leading edge". *EXPERIMENTS IN FLUIDS*, Vol. 55, No. 6. ISSN 0723-4864. doi:10.1007/s00348-014-1761-1.

Chen, J.H., Li, S.S. and Nguyen, T., 2012. "The effect of Leading Edge Protuberances on the performance of small aspect ratio foils". 15th International Symposium on Flow Visualization. doi:10.13140/RG.2.1.3716.7841.

Chen, WJ., Qiao, WY. and Wei, ZJ., 2020. "Aerodynamic performance and wake development of airfoils with wavy leading edges". *AEROSPACE SCIENCE AND TECHNOLOGY*, Vol. 106. ISSN 1270-9638. doi:10.1016/j.ast.2020.

106216.

Custodio, D., 2007. "The effect of humpback whale-like leading edge protuberances on hydrofoil performance". *Worcester Polytechnic Institute*, Vol. 75.

De paula, A., Meneghini, J., Kleine, V. and Girardi, R., 2017. "The wavy leading edge performance for a very thick airfoil". doi:10.2514/6.2017-0492.

De paula, A., Rios, A., Ferreira, P.H., Kleine, V. and Silva, R., 2018. "Swept wing effects on wavy leading edge phenomena". doi:10.2514/6.2018-4253.

Dropkin, A., Custodio, D., Henoch, CW. and Johari, H., 2012. "Computation of Flowfield Around an Airfoil with Leading-Edge Protuberances". *JOURNAL OF AIRCRAFT*, Vol. 49, No. 5, pp. 1345–1355. ISSN 0021-8669. doi:10.2514/1.C031675.

Favier, J., Pinelli, A. and Piomelli, U., 2012. "Control of the separated flow around an airfoil using a wavy leading edge inspired by humpback whale flippers". *COMPTES RENDUS MECANIQUE*, Vol. 340, No. 1-2, pp. 107–114. ISSN 1631-0721. doi:10.1016/j.crme.2011.11.004.

Fish, F., 1999. "Performance constraints on the maneuverability of flexible and rigid biological systems".

Fish, F.E. and Battle, J.M., 1995. "Hydrodynamic design of the humpback whale flipper". *Journal of Morphology*, Vol. 225, No. 1, pp. 51–60. doi:10.1002/jmor.1052250105.

Flores Mezarina, J., Garcia-Ribeiro, D., Bravo-Mosquera, P. and Cerón-M, H., 2019. "AERODYNAMIC EFFECTS OF ASYMMETRICAL LEADING EDGE PROTUBERANCES ON A RECTANGULAR WING". doi:10.26678/ABCM.COBEM2019.COB2019-1141.

Fonseca, W., Silva, R., Orselli, R., De paula, A. and Galdino da Silva, R., 2021. "Numerical study of airfoil with wavy leading edge at high Reynolds number regime". *Revista Facultad de Ingeniería*. doi:10.17533/udea.redin.20200474.

Hansen, KL., Kelso, RM. and Dally, BB., 2011. "Performance Variations of Leading-Edge Tubercles for Distinct Airfoil Profiles". *AIAA JOURNAL*, Vol. 49, No. 1, pp. 185–194. ISSN 0001-1452. doi:10.2514/1.J050631.

Hansen, KL., Rostamzadeh, N., Kelso, RM. and Dally, BB., 2016. "Evolution of the streamwise vortices generated between leading edge tubercles". *JOURNAL OF FLUID MECHANICS*, Vol. 788, pp. 730–766. ISSN 0022-1120. doi:10.1017/jfm.2015.611.

Hansen, K., Kelso, R. and Dally, B., 2010. "An investigation of three-dimensional effects on the performance of tubercles at low reynolds numbers". Conference: 17th Australasian Fluid Mechanics Conference.

Hassan, G., Hassan, A. and Youssef, M.E., 2015. "Numerical investigation of medium range re number aerodynamics characteristics for NACA0018 airfoil". *CFD Letters*, Vol. 6.

Johari, H., Henoch, C., Custodio, D. and Levshin, A., 2007. "Effects of leading-edge protuberances on airfoil performance". *AIAA JOURNAL*, Vol. 45, No. 11, pp. 2634–2642. ISSN 0001-1452. doi:10.2514/1.28497.

Joseph, J., Sridhar, S. and Alangar, S., 2019. "A comparison on the effect of leading edge tubercle on straight and swept wing at low reynolds number". Proc. of the 46th Nat. Conf. on Fluid Mechanics and Fluid Power (FMFP), Coimbatore (India), pp. 9–11.

Miklosovic, DS., Murray, MM. and Howle, LE., 2007. "Experimental evaluation of sinusoidal leading edges". *JOURNAL OF AIRCRAFT*, Vol. 44, No. 4, pp. 1404–1408. ISSN 0021-8669. doi:10.2514/1.30303.

Miklosovic, DS., Murray, MM., Howle, LE. and Fish, FE., 2004. "Leading-edge tubercles delay stall on humpback whale (Megaptera novaeangliae) flippers". *PHYSICS OF FLUIDS*, Vol. 16, No. 5, pp. L39–L42. ISSN 1070-6631. doi:10.1063/1.1688341.

Perez-Torro, R. and Kim, JW., 2017. "A large-eddy simulation on a deep-stalled aerofoil with a wavy leading edge". *JOURNAL OF FLUID MECHANICS*, Vol. 813, pp. 23–52. ISSN 0022-1120. doi:10.1017/jfm.2016.841.

Skillen, A., Revell, A., Pinelli, A., Piomelli, U. and Favier, J., 2015. "Flow over a wing with leading-edge undulations". *AIAA Journal*, Vol. 53, No. 2, pp. 464–472. doi:10.2514/1.J053142.

Steed, R., 2011. "High lift CFD simulations with an SST-Based predictive laminar to turbulent transition model". In *49th AIAA Aerospace Sciences Meeting Including the New Horizons Forum and Aerospace Exposition*. doi:10.2514/6.2011-864.

Watts, P., Fish, F.E. *et al.*, 2001. "The influence of passive, leading edge tubercles on wing performance". Proc. Twelfth Intl. Symp. Unmanned Untethered Submers. Technol.

Yang, PX., Zhu, YC. and Wang, JJ., 2023. "Effect of leading-edge tubercles on the flow over low-aspect-ratio wings at low Reynolds number". *THEORETICAL AND APPLIED MECHANICS LETTERS*, Vol. 13, No. 1. ISSN 2095-0349. doi:10.1016/j.taml.2022.100386.

9. RESPONSIBILITY NOTICE

The current authors are solely responsible for the printed material included in this paper.